




RESEARCH ARTICLE | JULY 11 2025

## How Laplace pressure reshapes local structure: Voronoi analysis of water and argon droplets

Pal Jedlovsky  ; Marcello Sega  



*J. Chem. Phys.* 163, 024709 (2025)

<https://doi.org/10.1063/5.0275651>



### Articles You May Be Interested In

Voronoi neighbor statistics of hard-disks and hard-spheres

*J. Chem. Phys.* (August 2005)

Voronoi cell analysis: The shapes of particle systems

*Am. J. Phys.* (June 2022)

Global and local Voronoi analysis of solvation shells of proteins

*J. Chem. Phys.* (August 2010)



The Journal of Chemical Physics

## Special Topics Open for Submissions

[Learn More](#)

# How Laplace pressure reshapes local structure: Voronoi analysis of water and argon droplets

Cite as: J. Chem. Phys. 163, 024709 (2025); doi: 10.1063/5.0275651

Submitted: 14 April 2025 • Accepted: 5 June 2025 •

Published Online: 11 July 2025



Pal Jedlovsky<sup>1</sup> and Marcello Sega<sup>2,a)</sup>

## AFFILIATIONS

<sup>1</sup> Department of Chemistry, Eszterhazy Karoly Catholic University, Leanyka utca 12, H-3300 Eger, Hungary

<sup>2</sup> Department of Chemical Engineering, University College London, London WC1E 7JE, United Kingdom

<sup>a)</sup> Author to whom correspondence should be addressed: [m.sega@ucl.ac.uk](mailto:m.sega@ucl.ac.uk)

## ABSTRACT

Curvature induces pressure differences across liquid–vapor interfaces and introduces corrections to surface tension that are described by classical thermodynamics in the macroscopic limit via the Tolman length. At the nanoscale, however, deviations from this behavior are difficult to interpret due to the nonlocal character of the stress tensor and the ambiguity in defining bulk phases. We address this by applying Voronoi tessellation to nanodroplets of argon and water to examine how curvature alters the local molecular structure. Unlike conventional density profiles—smeared out by capillary fluctuations—the Voronoi analysis yields a quasi-local geometric observable that can resolve curvature-induced changes in packing even near the molecular liquid surface. We find that inhomogeneity effects extend deep into the droplet interior. Using a simple classic thermodynamic framework to remap the droplet molecular volumes onto those of the flat interface, we find a collapse onto a single trend, suggesting that there are no specific curvature-induced changes beyond those implied by macroscopic thermodynamics. Remarkably, this collapse holds even for droplets smaller than those where classical approaches fail to extract a consistent Tolman length using local pressure tensor definitions.

© 2025 Author(s). All article content, except where otherwise noted, is licensed under a Creative Commons Attribution (CC BY) license (<https://creativecommons.org/licenses/by/4.0/>). <https://doi.org/10.1063/5.0275651>

## I. INTRODUCTION

A detailed picture of how curvature modifies the local structure of fluid interfaces is essential for understanding, designing, and controlling systems across biology, chemistry, physics, and engineering,<sup>1</sup> from nucleation, growth, and phase transitions to nanodroplet<sup>2</sup> and film stability<sup>3</sup> and static and dynamic wetting.<sup>4,5</sup> At the nanoscale, the macroscopic assumptions about bulk-phase separation and the nature of the pressure field become questionable, motivating the need for structural observables that remain meaningful when classical thermodynamic assumptions break down.

Classical thermodynamics relies on two core concepts: that of the equimolar dividing surface and the surface of tension. The equimolar surface is the surface at which the mass excess vanishes. For a spherical droplet, the equimolar radius,  $R_e$ , is usually defined implicitly through the following relation:

$$\int_0^{R_e} [\rho_L - \rho(r)] r^2 dr = \int_{R_e}^{\infty} [\rho(r) - \rho_V] r^2 dr. \quad (1)$$

The surface of tension is defined thermodynamically via excess quantities, ensuring the relation  $(p^L - p^V) \delta V = \gamma \delta A + C \delta R$ , where  $p^L$  and  $p^V$  denote the pressures in the two bulk phases, and  $\delta V$ ,  $\delta A$ , and  $\delta R$  are the volume, surface area, and curvature radius changes, respectively. The associated coefficients are the surface tension  $\gamma$  and the curvature coefficient  $C$ . Since  $\delta A / \delta V$  and  $\delta R / \delta V$  depend on different powers of the radius at which they are calculated, but the difference  $\Delta p = p^L - p^V$  does not, it follows that  $\gamma$  and  $C$  depend on the choice of the radius  $R$  used to locate the Gibbs dividing surfaces. The customary approach is then to define the specific Gibbs dividing surface known as the surface of tension of radius  $R_s$ , defined as the one for which the curvature term  $C \delta R$  vanishes, or, equivalently, for which the macroscopic Laplace pressure jump expression is formally recovered,<sup>6–8</sup>

$$\Delta p = \frac{2\gamma(R_s)}{R_s}, \quad (2)$$

where the dependence of  $\gamma$  on the surface of tension radius  $R_s$  has been made explicit.

As Tolman calculated, the surface tension of a curved interface can be related to that of a planar one,  $\gamma_\infty$ , via

$$\gamma(R_s) = \frac{\gamma_\infty}{1 + 2\delta/R_s} \simeq \gamma_\infty \left(1 - \frac{2\delta}{R_s}\right). \quad (3)$$

The Tolman length, defined as  $\delta = R_e - R_s$ , represents the separation between the radius of the surface of tension,  $R_s$ , and is typically of the order of the molecular size or less in magnitude, although its precise value is not easy to estimate. Measuring  $\delta$  accurately is complicated by a range of factors, such as whether the system involves droplets or cavitating bubbles, the nature of the interaction potentials (symmetric or asymmetric), how close the system is to the critical point, and whether particle-based or mesoscopic models are used.<sup>9–16</sup>

Tolman's original derivation is a thermodynamic approach that leaves out structural detail. As long as the bulk phases are well-defined, the surface of tension [defined by Eq. (2)] and the corresponding Tolman length can be seen simply as a geometrical consequence. However, even statistical mechanical treatments do not fully resolve this issue, since the concept of local stress lacks a well-defined definition.<sup>17</sup> Depending on how one calculates the local stress, the estimated position of the surface of tension can vary by about a molecular diameter, as shown by both theoretical and simulation-based studies.<sup>8,17,18</sup>

When the curvature approaches the scale of the bulk correlation length, additional effects may come into play. These include finite size corrections and changes in the molecular arrangement at the curved liquid–vapor interface. Under such conditions, the Tolman length might appear to vary with size. However, the concept of Tolman length itself begins to lose meaning in this limit, since it relies on having a clearly defined liquid bulk phase, which might no longer hold at this scale.

To better understand how curvature affects the structure of nanoscopic droplets, here we explore the changes in the volume of Voronoi cells as a structural marker for the effect of curvature. We show that even if a bulk phase cannot be identified, a classic thermodynamic framework can still be used to link back to the macroscopic limit, giving the opportunity to test where it holds and where it breaks down.

## II. METHODS

We performed molecular dynamics simulations of nanodroplets and planar slabs of water and argon, as depicted in Fig. 1. Water was modeled using the TIP4P/2005 potential,<sup>19</sup> while argon was modeled using the Lennard-Jones potential  $U_{LJ}(r) = 4\epsilon[(\sigma/r)^{12} - (\sigma/r)^6]$ , with parameters  $\sigma = 3.4$  Å and  $\epsilon = 0.9964$  kJ/mol (equivalent to 119.84 K).<sup>20</sup> The simulations were carried out in the NVT (canonical) ensemble using the Verlet integration algorithm<sup>21</sup> with a time step of 2 fs. The Nosé–Hoover<sup>22,23</sup> thermostat with a relaxation time of 0.5 ps was used to keep the temperature of the systems fluctuating around 90 and 300 K for argon and water, respectively. The long range contributions to both dispersion and electrostatic interactions were calculated using the smooth version of the particle mesh Ewald<sup>24</sup> method with a real-space cutoff of 13 Å and a relative value of the real space part of the potential at the cutoffs of  $10^{-3}$  and  $10^{-5}$  for the dispersion and electrostatic interactions, respectively. The treatment of long range dispersion corrections is especially important in the case of argon<sup>25</sup> but has a sizable impact

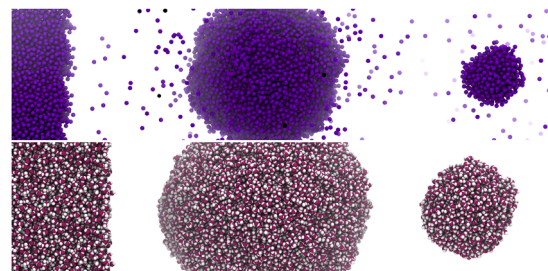


**FIG. 1.** Snapshots of the (from left to right) slab, largest and smallest droplets of (from top to bottom) argon and water. Only part of the simulation box is shown. Periodic copies of the slab in the vertical direction are shown.

also in water.<sup>26</sup> The molecular structure of water was kept rigid using the SETTLE algorithm.<sup>27</sup> Simulation boxes were chosen large enough for periodic image interaction to be minimal (yielding a 0.02% relative RMS force deviation for the largest water droplet system) and to ensure adequate vacuum padding in slab systems.

The number of molecules and simulation box edge lengths are summarized in Table I, along with the calculated average equimolar radii.

To distinguish liquid from vapor phase molecules, we used the DBSCAN (Density-Based Spatial Clustering of Applications with Noise) algorithm.<sup>28</sup> The search radius was set to 12 Å, and the threshold density for defining core points was determined automatically from the bimodal distribution of local densities, selecting the minimum between the liquid-like and vapor-like peaks.<sup>29</sup> Molecules forming the largest dense cluster were assigned to the liquid phase; all others were tagged as vapor.

The liquid–vapor interface was identified using the GITIM (Generalized Identification of Truly Interfacial Molecules) algorithm,<sup>30</sup> which generalizes the ITIM method<sup>31</sup> to arbitrarily shaped interfaces. GITIM performs a Delaunay triangulation of the centers of liquid-phase molecules and tags as interfacial those atoms that

**TABLE I.** Details of the simulation setups.

System	N	$\langle R_e \rangle$ (Å)	x and y edges (Å)	z edge (Å)
Ar drop	1 184	22.1	200.0	200.0
Ar drop	2 340	27.8	200.0	200.0
Ar drop	4 063	33.9	200.0	200.0
Ar drop	6 444	39.8	200.0	200.0
Ar drop	9 622	46.2	200.0	200.0
Ar drop	13 705	52.1	200.0	200.0
Ar slab	3 000	∞	36.01	216.1
H <sub>2</sub> O drop	1 903	23.7	150.0	150.0
H <sub>2</sub> O drop	3 738	29.7	150.0	150.0
H <sub>2</sub> O drop	6 457	35.7	150.0	150.0
H <sub>2</sub> O drop	10 276	41.7	150.0	150.0
H <sub>2</sub> O drop	15 337	47.7	150.0	150.0
H <sub>2</sub> O drop	21 877	53.7	150.0	150.0
H <sub>2</sub> O slab	4 320	∞	37.36	240.0

are the vertices of tetrahedra able to accommodate a probe sphere of a chosen radius. We have selected the probe radius as  $R_p = 2.0$  and  $2.2$  Å for argon and water, respectively, following the recipe that allows us to match the location of the equimolar dividing surface in flat interfaces.<sup>32</sup> In water, only oxygen atoms were considered in the determination of the interface and used as a proxy for the water molecule. Successive layers were assigned by repeatedly applying the GITIM algorithm. Both DBSCAN and GITIM were used as implemented in the Pytim package,<sup>33</sup> based on MDAAnalysis<sup>34</sup> and freely available at <https://github.com/Marcello-Sega/pytim>.

To probe molecular packing, we computed the Voronoi tessellation<sup>35,36</sup> of the atomic centers of the molecules in the liquid phase. The Voronoi tessellation is a space-filling partitioning of the simulation box in a set of polyhedra that is a generalization of the Wigner–Seitz cell<sup>37</sup> for disordered systems, with an illustrious history in the interpretation of the properties of liquids<sup>38–43</sup> and disordered packing in general,<sup>44</sup> including granular systems<sup>45</sup> and biological tissues,<sup>46</sup> but also as a tool for multiphysics simulations.<sup>47</sup>

The cell associated with a given molecule (here, we use the location of the argon and oxygen atoms as molecular centers) is a convex polyhedron whose internal points are closer to the molecule than to any other one. In practice, the faces of the polyhedra are bisecting planes of the segments connecting two neighboring molecules. Periodic boundary conditions were taken into account during tessellation to ensure consistent treatment of molecules at the box edges. We implemented a custom observable in the Pytim package to compute Voronoi-based statistics layer-by-layer, allowing us to associate each molecule with a well-defined local volume. Figure 2 reports the Voronoi tessellation of a two dimensional system for illustrative purposes. Note that in Fig. 2, we did not draw the large polyhedra associated with the particles located at the border of the droplet and defined through the particles in the periodic copies of the system.

Unlike the conventional density field, defined as  $\rho(\mathbf{r}) = \sum_i \langle \delta(\mathbf{r} - \mathbf{r}_i) \rangle$  (with the angular brackets denoting a canonical average) or its inverse—the local molecular volume—which are strictly local quantities, the corresponding Voronoi-based estimates

depend explicitly on the arrangement of a molecule and its neighbors. For this reason, we refer to them as quasi-local quantities. Recently, the Voronoi cells have been used in this way to define and analyze the quasi-local density in water droplets, as they allow us to bypass the large oscillations that characterize the conventional density profiles of droplets close to their center.<sup>48</sup>

In addition, we computed several thermodynamic quantities in the following way. We estimated the isothermal compressibility,

$$\kappa_T = -\frac{1}{V} \left( \frac{\partial V}{\partial p} \right)_{N,T}, \quad (4)$$

using the following fluctuation formula:<sup>49</sup>

$$\kappa_T = \frac{1}{k_B T} \frac{\langle \Delta V^2 \rangle}{\langle V \rangle}, \quad (5)$$

where  $k_B$  is Boltzmann's constant and  $T$  is the absolute temperature, from simulations of the bulk liquid in the NpT ensemble at the same state point as the slab systems. For the NpT simulations, we used a Parrinello–Rahman barostat<sup>50</sup> with a time constant of 4 ps. The planar surface tension  $\gamma_\infty$  was calculated from the slab simulations using the mechanical route  $\gamma_\infty = (p_N - p_T)/2L_z$ , where  $p_N$  and  $p_T$  are the normal and lateral pressure tensor elements, respectively, and  $L_z$  is the simulation box edge length in the direction perpendicular to the interface.

Finally, a straightforward calculation shows that, in a finite simulation box, the definition of the equimolar radius, Eq. (1), can be recast into the simpler explicit form

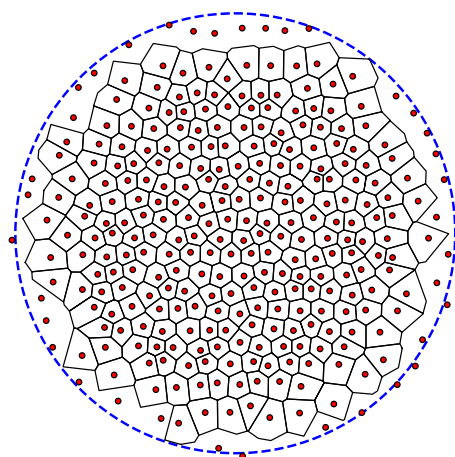
$$R_e^3 = \frac{3}{4\pi} \frac{N - \rho_V V}{(\rho_L - \rho_V)}, \quad (6)$$

where  $V$  is the simulation box volume and  $N$  is the total number of molecules in the simulation box.

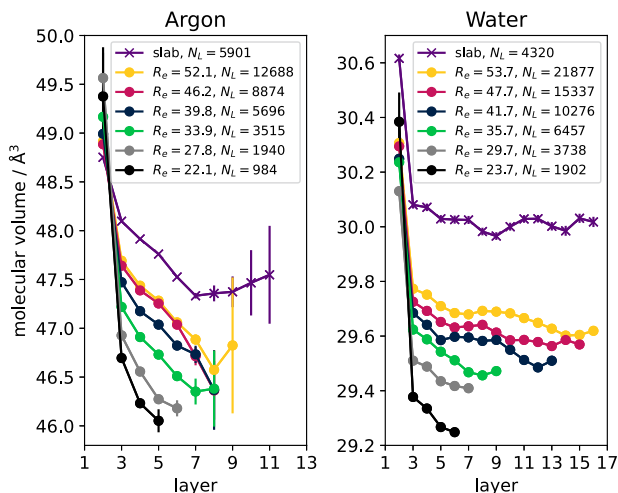
### III. RESULTS AND DISCUSSION

Figure 3 shows the layer-resolved average molecular volumes computed via Voronoi tessellation for nanodroplets and slabs of argon and water. The legend reports the equimolar radius of the droplet as well as the average number of molecules in the liquid phase,  $N_L$ , as determined by the DBSCAN procedure. To determine  $R_e$ , instead, we use its definition, Eq. (6), and estimate  $\rho_L = 1/v_L$  using the average Voronoi volume of atoms in the deepest resolved layer of each droplet, that is, the last one with acceptable statistics. This avoids invoking a bulk region, which cannot be consistently defined in small droplets. The vapor density  $\rho_V$  appearing in the denominator of Eq. (6) is negligible, but this is not the case, at least for argon at 90 K, for the term  $\rho_V V$  at the numerator ( $\rho_V$  is instead practically zero for water at 300 K), and so  $\rho_V$  has to be estimated from the number of molecules in the gas phase and its volume. The latter can be calculated as that of the simulation box with the exclusion of that occupied by the liquid—for which a rough estimate using  $\rho_L N_L$  is usually sufficient when, as in our case, the simulation box is much larger than the droplet.

The first data point shown corresponds to the second molecular layer, as Voronoi volumes in the outermost layer are ill-defined due to large voids and incomplete coordination shells, as depicted schematically in Fig. 2. Even in the second layer, particularly for



**FIG. 2.** An illustrative, two dimensional system in the shape of a circular droplet with local density decreasing when nearing the border. The Voronoi cell edges are reported as black lines.



**FIG. 3.** Molecular volumes determined via the Voronoi tessellation as a function of the molecular layer for argon (left panel) and water (right panel). Error bars represent one standard deviation and are, in some cases, smaller than the symbol. Layer 1 corresponds to the surface of the droplet/slab. The average distance between layers is 3.2 and 2.9 Å for argon and water, respectively.

small droplets, residual influence from these interfacial voids may persist. This is because the GITIM algorithm assigns atoms to layers based on a Delaunay triangulation, but it incorporates excluded volume effects through the atomic and probe sphere radii. As a result, it is not guaranteed that atoms labeled as “second layer” do not have any facet shared with large voids in the vapor phase. To avoid overinterpretation, here we do not draw conclusions from the second-layer data. From the third layer onward, instead, atoms are reliably shielded from the interface, and their Voronoi volumes reflect genuine local packing environments.

For both water and argon, the molecular volumes below the second layer are consistently smaller in the droplets than in the slabs. This effect becomes stronger with decreasing droplet size, consistent with curvature-induced compression. In argon, the molecular volumes decrease steadily with depth and appear to plateau, in the slab, only around the seventh or eighth layer. The droplets show no clear plateau or, at best, just a mild indication of the presence of a plateau. It is worth noting that while layers deeper than those reported in Fig. 3 did appear during the analysis, the number of atoms involved was so small that statistical noise rendered their average volumes unreliable, and we excluded them from the analysis.

Water exhibits a markedly different behavior. The change in molecular volume as a function of the layer is negligible if compared to argon, particularly so in the slab, but to a lesser extent also in the droplets. This decreased susceptibility to the pressure change could well be an effect of the greater structural rigidity provided by the hydrogen-bond network of water. Still, also in water droplets, the molecular volumes do not reach a plateau, with the possible exception of layer 12 and above.

These results highlight several important aspects of how curvature affects molecular packing in nanodroplets. First, the notion of a bulk-like liquid core breaks down even for droplets whose equimolar radius is one order of magnitude larger than the molecular size.

Second, the finite compressibility of the liquid emerges not only through the global dependence of volume on curvature radius but also through its layer-resolved variation as a function of depth, suggesting that the local molecular volume reflects a gradient in the local effective stress, driven by the reduced coordination and interaction experienced near the surface. Only atoms sufficiently deep in the droplet feel the full internal pressure imposed by curvature.

The question that arises now is to what extent the observed variations in molecular volume near the interface are due to curvature-induced pressure and to what extent they instead reflect intrinsic structural features of the liquid. Here, we use the term “intrinsic” to refer to structural effects that cannot be accounted for by a simple thermodynamic modeling. In other words, we aim to separate the contribution of Laplace pressure and compressibility from structural effects not captured by classical thermodynamics.

To this end, we adopt a strategy to link the change in molecular volume to the internal pressure via the isothermal compressibility  $\kappa_T$ . Under the assumption that the Voronoi volume serves as a proxy for the (inverse) local density, one can perform an expansion to first order in the inverse curvature radius around  $1/R_s = 0$ ,

$$v(R_s) - v_\infty = \left. \frac{\partial v}{\partial p} \right|_{p=p_\infty} [p^L(R_s) - p_\infty], \quad (7)$$

with  $p_\infty$  being the vapor pressure of the planar interface and  $v_\infty$  being the molecular (not the molar) volume of the liquid in the bulk of the planar interface. For our systems, the difference  $p^L(R_s) - p_\infty$  is practically indistinguishable from the Laplace pressure drop  $\Delta p = p^L(R_s) - p^V(R_s)$ . This can be seen from Kelvin’s equation,

$$\log \frac{p^V(R_s)}{p_\infty} = \frac{v_\infty}{k_B T} \left[ p^V(R_s) - p_\infty + \frac{2\gamma(R_s)}{R_s} \right]. \quad (8)$$

If the condition  $p_\infty v_\infty \ll k_B T$  is met, as it is in the present cases, then

$$p^V(R_s) \simeq p_\infty \exp \left[ \frac{2\gamma(R_s)}{R_s} \frac{v_\infty}{k_B T} \right]. \quad (9)$$

For both water and argon, the argument of the exponential function is roughly of the same order, for example, around about 0.4 for a 25 Å radius droplet, so that  $p^V \simeq 1.5p_\infty$  is at most of the order of magnitude of one bar. This is a much smaller value than the Laplace drop for such a droplet, about 120 and 600 bar for argon and water, respectively, so that  $p_\infty$  and  $p^V(R_s)$  can be used interchangeably in our equations, or, for that matter, disregarded.

The molecular volume change in Eq. (7) can then be expressed in terms of pressure drop using the definition of the compressibility as  $v(R_s) - v_\infty \simeq -v_\infty \kappa_T \Delta p$ . Using Laplace’s formula, we reach the expression

$$\frac{v(R_s)}{v_\infty} = 1 - \frac{2\kappa_T \gamma(R_s)}{R_s} = 1 - \frac{2\kappa_T \gamma_\infty}{R_e + \delta}. \quad (10)$$

We note in passing that the  $\kappa_T \gamma_\infty$  factor is similar to the analytical expression for the Tolman length proposed by Blockhuis and colleagues.<sup>12</sup>

Figure 4 presents the sampled molecular volumes rescaled by the volume ratio expected from purely thermodynamic effects,



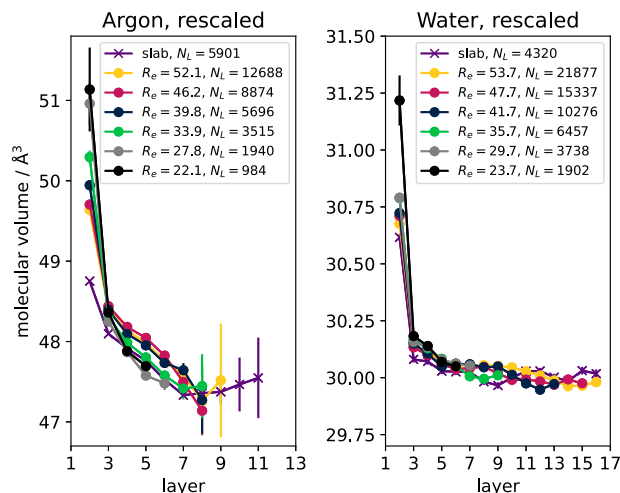


**FIG. 4.** Molecular volumes rescaled using Eq. (10) as a function of the molecular layer for argon (left panel) and water (right panel). Error bars represent one standard deviation and are, in some cases, smaller than the symbol. Layer 1 corresponds to the surface of the droplet/slab. The average distance between layers is 3.2 and 2.9 Å for argon and water, respectively.

Eq. (10) [i.e., we plot  $v(R_s)/[1 - 2\kappa_T\gamma_\infty/(R_e + \delta)]$ ], for droplets of various sizes, alongside the slab reference profiles. As values for the Tolman length of droplets, we used some recent estimates:  $\delta \simeq -0.34$  Å for argon<sup>51</sup> and  $\delta \simeq -0.5$  Å for water.<sup>15,52,53</sup> Here, we note that Eq. (10) is not particularly sensitive to the actual value of  $\delta$ , at least for the range of  $R_e$  values we investigated. Factorovich *et al.* found a similar lack of sensitivity in fitting Kelvin's equation as a function of the droplet size,<sup>54</sup> although they addressed much smaller droplets, down to the molecular cluster sizes. With the resolution of our data, thus, changing  $\delta$  by a factor of 2 does not affect the overall qualitative picture. Because of this, the expression for  $\delta$  that can be obtained by inverting Eq. (10) is not particularly useful.

In both argon and water, the molecular volume curves collapse well onto the slab reference one, confirming that the compressibility-based correction does, in fact, correctly capture the curvature-induced pressure, supporting the consistency of the thermodynamic framework we used to interpret curvature effects. Evident differences appear in the second layer, but as we mentioned already, this could well be an artifact of the method. Nevertheless, we find it striking that the inhomogeneity that characterizes the deeper layers can be so well reconciled by using the simple proposed thermodynamic rescaling.

It is also worth noting that the nanodroplets of argon studied here are all smaller than those for which Blockhuis and van Giessen observed a linear relationship between  $R_e\Delta p$  and  $1/R_e$ , consistent with a constant Tolman length.<sup>51</sup> This breakdown occurred precisely in the regime where the local pressure tensor becomes unreliable. In contrast, the analysis based on molecular volumes and their rescaling via macroscopic thermodynamic quantities bypasses this limitation and reveals a consistent structural response even at these high degrees of curvature.

#### IV. CONCLUSIONS

At the nanoscale, curvature effects are expected to play a relevant role in determining the behavior of liquid-vapor interfaces. However, it is currently unclear to what extent the changes induced by curvature are governed by purely thermodynamic effects and to what extent intrinsic structural changes such as curvature-dependent local structural rearrangement are involved. In this work, we addressed this problem by focusing on a structural observable: the molecular volume extracted from Voronoi tessellation. This quantity serves as a quasi-local probe of molecular packing and offers a way to assess how curvature modifies the internal structure of nanodroplets even in the absence of a clearly identifiable bulk phase.

We combined this geometric approach with a simple thermodynamic expression, in which changes in molecular volume are related to the Laplace pressure jump via the isothermal compressibility and surface tension. Using this framework, we rescaled the layer-resolved molecular volumes in argon and water droplets of varying sizes and compared them to the respective planar slab references. This approach enabled us to investigate the extent of the purely thermodynamic contribution of the Laplace pressure, providing the possibility to identify eventual intrinsic structural responses to curvature.

Our goal was not to estimate the Tolman length but to explore whether structural signatures—in particular, molecular volumes—reflect the expected response to the Laplace pressure. The rescaling of molecular volumes within a classical thermodynamic framework does indeed capture, with the exception of the first two layers, the overall behavior of the response of argon and water. The collapse of the rescaled volume curves on top of the flat interface ones indicates that the differences can be fully ascribed to the Laplace pressure drop and interpreted in terms of the usual thermodynamic framework only.

Note that our results do not exclude curvature-dependent effects on the Tolman length.<sup>2</sup> However, the collapse also happens for curvature radii that were previously beyond the reach of approaches relying on local pressure tensor definitions.<sup>12</sup>

The non-homogeneity of the local volumes within a single droplet, instead, most likely reflects the presence of a finite interaction range and the corresponding non-locality of quantities such as the energy or the stress tensor. We note in passing that this can, in fact, result in an implicit dependence of the surface tension on the size of the droplet beyond what Eq. (3) (with a size-independent Tolman length) describes, as the latter takes into account only the geometric effect.

It would be interesting to look more in detail at the origin of the increased molecular volume in the second layer. In water, there are indications that in the first two to three layers, the fraction of LDL-like water at 300 K is larger than in the bulk.<sup>48,55,56</sup> This would qualitatively explain the increased volume of the second layer, although a more quantitative justification is in order. The authors are not aware of any similar mechanism in argon, so no option can be excluded, and further investigations are in order.

#### ACKNOWLEDGMENTS

The authors acknowledge the use of the SIGH cluster at the UCL Chemical Engineering Department.

## AUTHOR DECLARATIONS

## Conflict of Interest

The authors have no conflicts to disclose.

## Author Contributions

**Pal Jedlovsky:** Conceptualization (supporting); Investigation (equal). **Marcello Sega:** Conceptualization (lead); Investigation (equal).

## DATA AVAILABILITY

The data that support the findings of this study are available from the corresponding author upon reasonable request.

## REFERENCES

- <sup>1</sup>H.-J. Butt, K. Graf, and M. Kappl, *Physics and Chemistry of Interfaces* (John Wiley & Sons, Weinheim, 2023).
- <sup>2</sup>J. Wen, D. Dini, H. Hu, and E. R. Smith, "Molecular droplets vs bubbles: Effect of curvature on surface tension and Tolman length," *Phys. Fluids* **33**, 072012 (2021).
- <sup>3</sup>J. N. Israelachvili, P. M. McGuiggan, and A. M. Homola, "Dynamic properties of molecularly thin liquid films," *Science* **240**, 189–191 (1988).
- <sup>4</sup>D. Bonn, J. Eggers, J. Indekeu, J. Meunier, and E. Rolley, "Wetting and spreading," *Rev. Mod. Phys.* **81**, 739–805 (2009).
- <sup>5</sup>B. Andreotti and J. H. Snoeijer, "Statics and dynamics of soft wetting," *Annu. Rev. Fluid Mech.* **52**, 285–308 (2020).
- <sup>6</sup>R. C. Tolman, "Consideration of the Gibbs theory of surface tension," *J. Chem. Phys.* **16**, 758–774 (1948).
- <sup>7</sup>J. G. Kirkwood and F. P. Buff, "The statistical mechanical theory of surface tension," *J. Chem. Phys.* **17**, 338–343 (1949).
- <sup>8</sup>J. S. Rowlinson and B. Widom, *Molecular Theory of Capillarity* (Dover Publications, Inc., Mineola, NY, 2002).
- <sup>9</sup>M. P. A. Fisher and M. Wortis, "Curvature corrections to the surface tension of fluid drops: Landau theory and a scaling hypothesis," *Phys. Rev. B* **29**, 6252 (1984).
- <sup>10</sup>N. Bruot and F. Caupin, "Curvature dependence of the liquid-vapor surface tension beyond the Tolman approximation," *Phys. Rev. Lett.* **116**, 056102 (2016).
- <sup>11</sup>G. Menzl, M. A. Gonzalez, P. Geiger, F. Caupin, J. L. F. Abascal, C. Valeriani, and C. Dellago, "Molecular mechanism for cavitation in water under tension," *Proc. Natl. Acad. Sci. U. S. A.* **113**, 13582–13587 (2016).
- <sup>12</sup>E. M. Blokhuis and J. Kuipers, "Thermodynamic expressions for the Tolman length," *J. Chem. Phys.* **124**, 074701 (2006).
- <sup>13</sup>B. J. Block, S. K. Das, M. Oettel, P. Virnau, and K. Binder, "Curvature dependence of surface free energy of liquid drops and bubbles: A simulation study," *J. Chem. Phys.* **133**, 154702 (2010).
- <sup>14</sup>K. Binder, B. J. Block, P. Virnau, and A. Tröster, "Beyond the van der Waals loop: What can be learned from simulating Lennard-Jones fluids inside the region of phase coexistence," *Am. J. Phys.* **80**, 1099–1109 (2012).
- <sup>15</sup>M. N. Joshiak, R. Do, M. F. Doherty, and B. Peters, "Energetic and entropic components of the Tolman length for mW and TIP4P/2005 water nanodroplets," *J. Chem. Phys.* **145**, 204703 (2016).
- <sup>16</sup>M. Lulli, L. Biferale, G. Falcucci, M. Sbragaglia, and X. Shan, "Mesoscale perspective on the Tolman length," *Phys. Rev. E* **105**, 015301 (2022).
- <sup>17</sup>P. Schofield and J. R. Henderson, "Statistical mechanics of inhomogeneous fluids," *Proc. R. Soc. A* **379**, 231–246 (1982).
- <sup>18</sup>M. Sega, B. Fábán, and P. Jedlovsky, "Pressure profile calculation with mesh Ewald methods," *J. Chem. Theory Comput.* **12**, 4509–4515 (2016).
- <sup>19</sup>J. L. F. Abascal and C. Vega, "A general purpose model for the condensed phases of water: TIP4P/2005," *J. Chem. Phys.* **123**, 234505 (2005).
- <sup>20</sup>L. A. Rowley, D. Nicholson, and N. G. Parsonage, "Monte Carlo grand canonical ensemble calculation in a gas-liquid transition region for 12-6 Argon," *J. Comput. Phys.* **17**, 401–414 (1975).
- <sup>21</sup>M. P. Allen and D. J. Tildesley, *Computer Simulation of Liquids* (Oxford University Press, 2017).
- <sup>22</sup>S. Nosé, "A molecular dynamics method for simulations in the canonical ensemble," *Mol. Phys.* **52**, 255–268 (1984).
- <sup>23</sup>W. G. Hoover, "Canonical dynamics: Equilibrium phase-space distributions," *Phys. Rev. A* **31**, 1695–1697 (1985).
- <sup>24</sup>U. Essmann, L. Perera, M. L. Berkowitz, T. Darden, H. Lee, and L. G. Pedersen, "A smooth particle mesh Ewald method," *J. Chem. Phys.* **103**, 8577–8593 (1995).
- <sup>25</sup>P. J. in 't Veld, A. E. Ismail, and G. S. Grest, "Application of Ewald summations to long-range dispersion forces," *J. Chem. Phys.* **127**, 144711 (2007).
- <sup>26</sup>M. Sega and C. Dellago, "Long-range dispersion effects on the water/vapor interface simulated using the most common models," *J. Phys. Chem. B* **121**, 3798–3803 (2017).
- <sup>27</sup>S. Miyamoto and P. A. Kollman, "Settle: An analytical version of the SHAKE and RATTLE algorithm for rigid water models," *J. Comput. Chem.* **13**, 952–962 (1992).
- <sup>28</sup>M. Ester, H.-P. Kriegel, J. Sander, and X. Xu, "A density-based algorithm for discovering clusters in large spatial databases with noise," in *Proceedings of the 2nd International Conference on Knowledge Discovery and Data Mining (KDD-96)* (AAAI, 1996), Vol. 96, p. 226.
- <sup>29</sup>M. Sega and G. Hantal, "Phase and interface determination in computer simulations of liquid mixtures with high partial miscibility," *Phys. Chem. Chem. Phys.* **19**, 18968–18974 (2017).
- <sup>30</sup>M. Sega, S. S. Kantorovich, P. Jedlovsky, and M. Jorge, "The generalized identification of truly interfacial molecules (ITIM) algorithm for nonplanar interfaces," *J. Chem. Phys.* **138**, 044110 (2013).
- <sup>31</sup>L. B. Pártay, G. Hantal, P. Jedlovsky, Á. Vincze, and G. Horvai, "A new method for determining the interfacial molecules and characterizing the surface roughness in computer simulations. Application to the liquid-vapor interface of water," *J. Comput. Chem.* **29**, 945–956 (2008).
- <sup>32</sup>G. Hantal, P. Jedlovsky, and M. Sega, "Local structure of liquid/vapour interfaces approaching the critical point," *Soft Matter* **19**, 3773–3782 (2023).
- <sup>33</sup>M. Sega, G. Hantal, B. Fábán, and P. Jedlovsky, "Pytim: A python package for the interfacial analysis of molecular simulations," *J. Comput. Chem.* **39**, 2118–2125 (2018).
- <sup>34</sup>N. Michaud-Agrawal, E. J. Denning, T. B. Woolf, and O. Beckstein, "MDAnalysis: A toolkit for the analysis of molecular dynamics simulations," *J. Comput. Chem.* **32**, 2319–2327 (2011).
- <sup>35</sup>G. Voronoi, "Nouvelles applications des paramètres continus à la théorie des formes quadratiques. Deuxième mémoire. Recherches sur les paralléloèdres primitifs," *J. Reine Angew. Math.* **1908**, 198–287.
- <sup>36</sup>F. Aurenhammer, "Voronoi diagrams—A survey of a fundamental geometric data structure," *ACM Comput. Surv.* **23**, 345–405 (1991).
- <sup>37</sup>C. Kittel and P. McEuen, *Introduction to Solid State Physics* (John Wiley & Sons, New York, 2018).
- <sup>38</sup>J. Finney, "Random packings and the structure of simple liquids. I. The geometry of random close packing," *Proc. R. Soc. A* **319**, 479–493 (1970).
- <sup>39</sup>F. H. Stillinger, "Structure in aqueous solutions of nonpolar solutes from the standpoint of scaled-particle theory," in *The Physical Chemistry of Aqueous System: A Symposium in Honor of Henry S. Frank on His Seventieth Birthday* (Springer US, Boston, MA, 1973), pp. 43–60.
- <sup>40</sup>V. A. Luchnikov, N. N. Medvedev, A. Appelhagen, and A. Geiger, "Medium-range structure of amorphous silicon studied by the Voronoi–Delaunay method," *Mol. Phys.* **88**, 1337–1348 (1996).
- <sup>41</sup>G. Ruocco, M. Sampoli, A. Torcini, and R. Vallauri, "Molecular dynamics results for stretched water," *J. Chem. Phys.* **99**, 8095–8104 (1993).
- <sup>42</sup>M. G. Alinchenko, A. V. Anikeenko, N. N. Medvedev, V. P. Voloshin, M. Mezei, and P. Jedlovsky, "Morphology of voids in molecular systems. A Voronoi–Delaunay analysis of a simulated DMPC membrane," *J. Phys. Chem. B* **108**, 19056–19067 (2004).
- <sup>43</sup>A. Idrissi, P. Damay, K. Yukichi, and P. Jedlovsky, "Self-association of urea in aqueous solutions: A Voronoi polyhedron analysis study," *J. Chem. Phys.* **129**, 164512 (2008).
- <sup>44</sup>S. Torquato and F. H. Stillinger, "Jammed hard-particle packings: From Kepler to Bernal and beyond," *Rev. Mod. Phys.* **82**, 2633–2672 (2010).

- <sup>45</sup>S. V. Anishchik and N. N. Medvedev, "Three-dimensional Apollonian packing as a model for dense granular systems," *Phys. Rev. Lett.* **75**, 4314–4317 (1995).
- <sup>46</sup>M. Bock, A. K. Tyagi, J.-U. Kreft, and W. Alt, "Generalized Voronoi tessellation as a model of two-dimensional cell tissue dynamics," *Bull. Math. Biol.* **72**, 1696–1731 (2010).
- <sup>47</sup>R. I. Saye and J. A. Sethian, "The Voronoi implicit interface method for computing multiphase physics," *Proc. Natl. Acad. Sci. U. S. A.* **108**, 19498–19503 (2011).
- <sup>48</sup>S. M. A. Malek, P. H. Poole, and I. Saika-Voivod, "Thermodynamic and structural anomalies of water nanodroplets," *Nat. Commun.* **9**, 2402 (2018).
- <sup>49</sup>J. P. Hansen and I. R. McDonald, *Theory of Simple Liquids: With Applications to Soft Matter* (Elsevier Science, 2013).
- <sup>50</sup>M. Parrinello and A. Rahman, "Polymorphic transitions in single crystals: A new molecular dynamics method," *J. Appl. Phys.* **52**, 7182–7190 (1981).
- <sup>51</sup>A. E. van Giessen and E. M. Blokhuis, "Direct determination of the Tolman length from the bulk pressures of liquid drops via molecular dynamics simulations," *J. Chem. Phys.* **131**, 164705 (2009).
- <sup>52</sup>M. N. Joswiak, N. Duff, M. F. Doherty, and B. Peters, "Size-dependent surface free energy and Tolman-corrected droplet nucleation of TIP4P/2005 water," *J. Phys. Chem. Lett.* **4**, 4267–4272 (2013).
- <sup>53</sup>Ø. Wilhelmsen, D. Bedeaux, and D. Reguera, "Communication: Tolman length and rigidity constants of water and their role in nucleation," *J. Chem. Phys.* **142**, 171103 (2015).
- <sup>54</sup>M. H. Factorovich, V. Molinero, and D. A. Scherlis, "Vapor pressure of water nanodroplets," *J. Am. Chem. Soc.* **136**, 4508–4514 (2014).
- <sup>55</sup>A. Gorfer, C. Dellago, and M. Sega, "High-density liquid (HDL) adsorption at the supercooled water/vapor interface and its possible relation to the second surface tension inflection point," *J. Chem. Phys.* **158**, 054503 (2023).
- <sup>56</sup>P. Jedlovsky, C. Dellago, and M. Sega, "Hydrogen bond topology reveals layering of LDL-like and HDL-like water at its liquid/vapor interface," *J. Chem. Phys.* **163**, 024511 (2025).